THE JOURNAL OF BIOLOGICAL CHEMISTRY VOL. 284, NO. 13, pp. 8596–8604, March 27, 2009

Versican/PG-M Assembles Hyaluronan into Extracellular Matrix and Inhibits CD44-mediated Signaling toward Premature Senescence in Embryonic Fibroblasts*[S]

Received for publication, September 8, 2008, and in revised form, January 6, 2009 Published, JBC Papers in Press, January 21, 2009, DOI 10.1074/jbc.M806927200

Keittisak Suwan[‡§1], **Kanyamas Choocheep**[‡§1], **Sonoko Hatano**[‡], **Prachya Kongtawelert**[§], **Koji Kimata**[‡], **and Hideto Watanabe**[‡2]

From the [‡]*Institute for Molecular Science of Medicine, Aichi Medical University, Nagakute, Aichi 480-1195, Japan and the* [§]*Department of Biochemistry, Faculty of Medicine, Thailand Excellence Center for Tissue Engineering, Chiang Mai University, Chiang Mai 50200, Thailand*

Versican/PG-M is a large chondroitin sulfate proteoglycan of the extracellular matrix which interacts with hyaluronan at the N-terminal G1 domain, composed of A, B, and B′ subdomains. Recently, we generated knock-in mice *Cspg2*$^{\Delta3/\Delta3}$, whose versican, without the A subdomain, has decreased hyaluronan (HA) binding affinity, thereby exhibiting reduced deposition of versican in the extracellular matrix. Here, we show that the *Cspg2*$^{\Delta3/\Delta3}$ fibroblasts within 20 passages proliferate more slowly and acquire senescence. Whereas the extracellular matrix of the wild type fibroblasts exhibited a network structure of hyaluronan and versican, that of the *Cspg2*$^{\Delta3/\Delta3}$ fibroblasts exhibited ~35 and ~85% deposition of versican and HA, without such a structure. The *Cspg2*$^{\Delta3/\Delta3}$ fibroblasts showed a substantial increase of ERK1/2 phosphorylation and expression of senescence markers p53, p21, and p16. Treatment of wild type fibroblasts with hyaluronidase and exogenous hyaluronan enhanced ERK1/2 phosphorylation, and treatment with an anti-CD44 antibody that blocks HA-CD44 interaction inhibited the phosphorylation. These results demonstrate that versican is essential for matrix assembly involving hyaluronan and that diminished versican deposition increases free hyaluronan fragments that interact with CD44 and increase phosphorylation of ERK1/2, leading to cellular senescence.

The extracellular matrix (ECM)[3] not only supports cells and imparts architecture characteristic of individual tissues but also regulates cell behavior by storing and distributing cytokines and growth factors to target cells. Proper functioning of the ECM requires an elaborate matrix assembly that involves various ECM molecules, including collagens, proteoglycans, hyaluronan (HA), and glycoproteins. An alteration of the ECM structure may transmit a signal to cells and change their behavior.

Versican/PG-M (1, 2) is a large chondroitin sulfate (CS) proteoglycan of the ECM, synthesized mainly by fibroblasts and vascular smooth muscle cells. Its core protein consists of two globular domains G1 and G3 at the N and C termini, respectively, and two CS attachment domains CSα and CSβ between the two globular domains. Up to 23 CS chains are attached to these domains, and the molecular mass of versican reaches 1,000 kDa. The N-terminal G1 domain consists of A, B, and B′ looped subdomains. The B-B′ stretch binds HA, and the A subdomain enhances the binding (3). The C-terminal G3 domain binds other ECM molecules (4), including fibrillins (5), fibulin-1 (6), fibulin-2 (7), tenascins (8–10), type I collagen (11), and fibronectin (11). By interacting with these molecules, versican is incorporated into the ECM and serves as a structural macromolecule.

Versican exhibits two distinct expression patterns. Whereas it is constitutively expressed in adult tissues such as dermis and blood vessels and serves as a structural macromolecule of the ECM, versican is transiently expressed at high levels in various embryonic tissues and regulates cell behavior such as adhesion (12–14), migration (15–17), proliferation (18–20), and differentiation (21, 22). The G3 domain of versican has been shown to enhance proliferation of NIH3T3 fibroblasts via epidermal growth factor (EGF)-like motifs (23). The G3 domain without the EGF-like motifs enhances interaction of EGF receptor (EGFR) and β1-integrin, impairing growth of U87 astrocytoma cells (22). The V1 variant enhances proliferation and inhibits apoptosis of NIH3T3 fibroblasts, whereas the V2 variant exhibits an opposite activity (20). Although several lines of evidence showing the direct effects of versican domains have been provided, the precise mechanisms by which versican regulates cell behavior have not been fully understood.

Recently, we generated knock-in mice (*Cspg2*$^{\Delta3/\Delta3}$) whose versican lacks the A subdomain of the G1 domain.[4] These mice express the mutant versican at certain levels dependent on tis-

* This work was supported by Grants-in-aid for Scientific Research B and C KAKENHI (to H. W.) and Grants-in-aid for Priority Areas (to H. W.). The costs of publication of this article were defrayed in part by the payment of page charges. This article must therefore be hereby marked "*advertisement*" in accordance with 18 U.S.C. Section 1734 solely to indicate this fact.

[S] The on-line version of this article (available at http://www.jbc.org) contains supplemental Figs. S1 and S2.

[1] Both authors contributed equally to this work.

[2] To whom correspondence should be addressed: Karimata 21, Yazako, Nagakute, Aichi-gun, Aichi 480-1195, Japan. Tel.: 81-561-62-3311, Ext. 2086; Fax: 81-561-63-3532; E-mail: wannabee@aichi-med-u.ac.jp.

[3] The abbreviations used are: ECM, extracellular matrix; CS, chondroitin sulfate; HA, hyaluronan; EGF, epidermal growth factor; EGFR, EGF receptor; MAPK, mitogen-activated protein kinase; ERK, extracellular signal-regulated kinase; WT, wild type; FBS, fetal bovine serum; DMEM, Dulbecco's modified Eagle's medium; BrdUrd, bromodeoxyuridine; RTK, receptor tyrosine kinase; PBS, phosphate-buffered saline; JNK, c-Jun N-terminal kinase; MEK, MAPK/ERK kinase.

[4] S. Hatano, K. Kimata, N. Hiraiwa, M. Kusakabe, E. Adachi, Z. Isogai, T. Shinomura, and H. Watanabe, submitted for publication.

sue types as compared with the level of normal versican in WT mice. The knock-in mice exhibit abnormalities in cardiovascular systems and skin, contrasting to versican-null *hdf* mice, which die at embryonic day 9.5 from severe cardiac defects (24). Because *hdf* heterozygotes expressing ~50% normal versican are viable, the abnormalities of *Cspg2*$^{\Delta 3/\Delta 3}$embryos are likely due to decreased deposition of the mutant versican without the A subdomain in the ECM. Thus, analysis of *Cspg2*$^{\Delta 3/\Delta 3}$ mice leads to elucidation of the functions of versican in the ECM, distinct from those of transiently expressed versican.

To further investigate the role of versican in the ECM, we characterized embryonic fibroblasts obtained from *Cspg2*$^{\Delta 3/\Delta 3}$ mice. These cells exhibited characteristics of senescence within 20 passages. Analysis of matrix assembly, phosphorylation of MAPKs, and expression of senescence markers suggested that disruption of the HA network structure by decreased versican deposition caused constitutive ERK1/2 phosphorylation via CD44 and led to premature senescence. These results demonstrate that versican regulates HA- and CD44-mediated signal transduction in the extracellular matrix.

EXPERIMENTAL PROCEDURES

Cell Culture—Fibroblasts were prepared three times from embryos at embryonic day 12.5 obtained by mating heterozygote mice as described previously (25). Three batches, M1, M2, and M3, of *Cspg2*$^{\Delta 3/\Delta 3}$ and wild type (WT) fibroblasts from the same littermates were used. The cells were grown in DMEM supplemented with 10% FBS, penicillin (100 μg/ml), and streptomycin (100 μg/ml), at 37 °C, 5% CO_2, 95% air. The cells were genotyped by PCR. NIH3T3 cells were maintained in DMEM containing 10% FBS, penicillin, and streptomycin.

Cell Proliferation Assay—The cell proliferation rate was measured using a BrdUrd enzyme-linked immunosorbent assay cell proliferation assay (Roche Applied Science). Two thousand cells were plated in 96-well plates, cultured overnight, and then incubated with 10 μM BrdUrd labeling solution (100 μl) for 2 h at 37 °C. DMEM containing 10% FBS was used as a negative control. The solution was removed, and then the cells were fixed with 200 μl of cell-fixing solution for 30 min at 25 °C and incubated with 100 μl of a peroxidase-conjugated anti-BrdUrd monoclonal antibody for 90 min at 25 °C. The solution was removed and washed three times using 300 μl of washing solution. TMB substrate solution (100 μl/well, KPL) was added and incubated at 25 °C, and then the reaction was terminated with 25 μl of 1 M HCl. The absorbance in each well was measured directly using a spectrophotometric microplate reader at a test wavelength of 450 nm and a reference wavelength of 690 nm. This measures the degree of cell proliferation.

For the cell count assay, fibroblasts (1×10^5 cells) were plated onto 6-well plates and cultured in DMEM containing 10% FBS. The cell number was counted at days 1–6, using a hemocytometer. Statistical analysis was performed using Student's *t* test. The apoptotic levels of cells were measured using the Apodirect *in situ* DNA fragmentation kit (Biovision) according to the manufacturer's instructions.

β-Galactosidase Staining—Staining of cells for β-galactosidase was performed as previously described (26). Briefly, cells were washed in PBS and fixed in 2% formaldehyde for 3 min at room temperature. After washing, the cells were incubated for 12 h at 37 °C without CO_2 in freshly prepared staining buffer containing 1 mg/ml 5-bromo-4-chloro-3-indoyl β-D-galactoside in 0.1 M citric acid and 0.2 M sodium phosphate solution, pH 6.0, 5 mM potassium ferricyanide, 5 mM potassium ferrocyanide, 150 mM NaCl, and 2 mM $MgCl_2$. The cells were then observed and photographed under a light microscope.

Immunocytochemistry—The cells were cultured in DMEM containing 10% FBS in Lab-Tek II chamber slides (Nalgen Nunc International) and fixed in 10% buffered formalin. The chamber slides were immunostained with the following specific antibodies: rabbit polyclonal anti-versican CS-α and CS-β (a mixture of ×1000 dilutions) (27), rabbit polyclonal anti-laminin (×1000) (28), rabbit polyclonal anti-fibronectin (×1000) (29), and rat monoclonal anti-CD44 (clone IM7.8.1, Acris, 5 μg/ml). An anti-rabbit IgG conjugated with horseradish peroxidase (×1000; Dako) was used as the secondary antibody. For detection of HA, cultured slides were fixed with 10% buffered formalin for 30 min, blocked in 1% bovine serum albumin for 1 h at room temperature, and then treated with 2 μg/ml biotinylated HA-binding protein (Seikagaku Corp.) for 2 h at room temperature. After washing three times with PBS, streptavidin-horseradish peroxidase was added, and the slide was incubated at room temperature for 15 min. After washing three times with PBS, the slide was treated with DAB solution (DAKO) to develop color. In some experiments, anti-rat IgG-488 and streptavidin 594 (Alexa) were used in place of horseradish peroxidase-conjugated anti-rat antibody and streptavidin, for immunofluorescent staining.

Immunoblot Analysis—The cells were lysed in 50 mM Tris-HCl, 2 mM EDTA, 2 mM EGTA, 150 mM NaCl, 2% Triton X-100, and protease inhibitors (Protease inhibitor mixture tablets; Roche Applied Science). The cell lysate was centrifuged at 13,000 × *g* for 10 min at 4 °C. Protein concentration was determined using the BCA assay (Pierce), and the sample at an equal protein amount was subjected to SDS-PAGE under a reducing condition. The proteins were electrotransferred to a polyvinylidene difluoride membrane, and the membrane was soaked in 5% skim milk in PBS containing 0.1% Tween 20 for blocking. The membrane was treated with antibodies at 4 °C overnight. The primary antibodies against MAPKs and their phosphorylation forms and p53 were from Cell Signaling, and the antibody against actin was from Sigma. After washing three times with PBS containing 0.1% Tween 20, the membrane was treated with corresponding secondary antibodies at room temperature for 1 h. After washing three times as above, the signal was detected with ECL reagents (Amersham Biosciences). When necessary, the blots were stripped in stripping buffer (Restore™ Western blot stripping buffer; Pierce), and the membrane was used for immunoblot analysis using another antibody.

CS Chain Analysis—The cells were cultured in 60-mm culture dishes up to confluence, and the cell lysate prepared by a Cytobuster reagent (Novagens) was subjected to centrifugation at 13,000 × *g* 4 °C for 10 min. The supernatant was applied to a 0.3 ml of DEAE-Sephacel column equilibrated with the equilibration buffer (50 mM Tris-HCl, pH 7.2, 0.1 M NaCl). After washing with 3 ml of equilibration buffer, proteoglycan fraction was eluted with elution buffer (50 mM Tris-HCl, pH 7.2, 2 M

NaCl). Three volumes of 95% ethanol containing 1.3% potassium acetate were added to the eluate, and the solution was chilled at −20 °C overnight and centrifuged at 13,000 × *g* for 30 min at 4 °C. Protein concentration in the proteoglycan precipitate was determined by BCA assay. An equal amount of proteoglycan was dissolved in chondroitinase ABC buffer (20 mM Tris-HCl, pH 8.0, 20 mM sodium acetate, 0.02% bovine serum albumin), digested with chondroitinase ABC (5 milliunits/ml) at 37 °C for 3 h, and then the reaction was stopped by boiling at 100 °C for 5 min. The unsaturated CS disaccharide product was analyzed by fluorometric postcolumn high performance liquid chromatography as described previously (27).

Real Time Reverse Transcription-PCR—Poly(A) RNA was prepared from cultured fibroblasts using a MicroFast Track™ kit (Invitrogen), and cDNA was reverse-transcribed using a SuperScript III first strand synthesis system (Invitrogen). PCR was performed using the TaqMan Prism 7700 (Applied Biosystems). The sequences of the probe and a set of primers for mouse versican were the following: forward primer, 5′-CCAGTGTGAACTTGATTTTGATGAA-3′; reverse primer, 5′-AACATAACTTGGGAGACAGAGACATCT-3′; TaqMan probe, 5′-CACTCTAACCCTTGTCGGAATGGT-3′. PCR was similarly performed using a set of the probe and primers for rodent glyceraldehyde-3-phosphate dehydrogenase (Applied Biosystems).

Quantification of Hyaluronan—For the HA assay, at confluence, the conditioned medium was collected, and cells were placed in 0.5 ml of 0.15 M Tris-HCl, pH 7.3, 0.15 M NaCl, 10 mM $CaCl_2$, and 5 mM deferoxamine mesylate containing 10 units of protease K and incubated for 2 h at 55 °C. The sample was centrifuged at 14,000 × *g* for 25 min at 4 °C, and the supernatant was analyzed. HA concentrations were measured using sandwich enzyme-linked immunosorbent assay. Microtiter plates were coated with 50 μl of 0.25 μg/ml HA-binding protein at 4 °C overnight and then blocked with 2% bovine serum albumin in PBS-Tween for 1 h at 37 °C. To each well, the samples or various concentrations of HA (HA standards) were added and incubated for 1 h at 37 °C, and then a biotinylated HA-binding protein solution was added. After incubation, the plate was washed and further incubated with peroxidase-conjugated streptavidin. Finally, a color was developed, the reaction was stopped with 1 M HCl, and absorbance was measured at 450 nm.

Treatment with EGF and PD98059—Fibroblasts (2×10^5) were grown up to confluence, and then the culture medium was replaced with DMEM containing 1% FBS and further cultured. The cells were treated with EGF (20 mg/ml) for 2 h or with PD98059 (30 mM) for 1 h, and at 18 h, the cells were collected and used for immunoblot analysis.

Treatment with an Anti-CD44 Antibody, Hyaluronidase, and Hyaluronan—Fibroblasts (2×10^5) were grown in chamber slides for 24 h, and then the culture medium was changed to 1% FBS and further grown for 18 h. An anti-CD44 monoclonal antibody KM81 that blocks HA-CD44 interaction (Cedar Lane Laboratories) or IM7 (Acris) that does not was added to cultured fibroblasts at final concentrations of 1 and 5 μg/ml. The cells were cultured for 1 h and fixed with 4% paraformaldehyde for 10 min at room temperature. After washing with PBS, the cells were permeabilized with 0.2% Triton X-100 in PBS for 2 min at room temperature, blocked with 0.2% gelatin in PBS for 1 h, and then incubated with an anti-phospho-ERK1/2 (×300, Cell signaling) at 4 °C overnight. After washing in PBS, the cells were stained with Alexafluoro594-conjugated secondary antibody (×1000; Molecular Probes) for 1 h at room temperature, washed with PBS, mounted on slides, and observed using a confocal microscope (Zeiss).

For hyaluronidase treatment, the WT fibroblasts at confluence in 6-well plates were used. The medium was replaced with fresh medium containing 1% FBS, and the cells were cultured for 18 h. Then bovine testicular hyaluronidase (Sigma) at final concentrations of 0.2 and 2 mg/ml was added, and the cells were cultured for 30 min and 2 h. Cell lysates were collected and applied to immunoblot analysis for phospho-ERK1/2, ERK1/2, and actin, as described above. In other experiments, the cultures were treated with 0.2 or 2 mg/ml hyaluronidase alone or together with 5 μg/ml anti-CD44 antibody for 2 h, followed by immunoblot analysis as described above. For HA treatment, the medium was replaced with a fresh medium without serum and cultured for 2 h. Then HA with molecular sizes of 1,000, 104, and 8.2 kDa, at final concentrations of 5, 50, and 150 μg/ml were added, the cells were cultured for 16 h, and the cell lysates were applied to immunoblot analysis.

RESULTS

$Cspg2^{\Delta 3/\Delta 3}$ Fibroblasts Proliferate Slowly at Early Passages—Initially, we attempted to generate versican (*Cspg2*)-null mice using conventional technology with a targeting vector such that the PGK promoter-driven neo^r gene was inserted into exon 3 encoding the A subdomain of the G1 domain (supplemental Fig. S1). Whereas the heterozygote mice $Cspg2^{+/\Delta 3}$ were viable and fertile, the homozygote $Cspg2^{\Delta 3/\Delta 3}$ mice were embryonically lethal.[4] We isolated fibroblasts from WT and $Cspg2^{\Delta 3/\Delta 3}$ embryos at embryonic day 12.5 and examined the expression of versican. Contrary to our expectations, immunoblot analysis revealed expression of the versican core protein (data not shown). Analysis of mRNA revealed skipping exon 3, resulting in the "in-frame" synthesis of versican without the A subdomain (data not shown).

Then we investigated the role of versican without the A subdomain using $Cspg2^{\Delta 3/\Delta 3}$ fibroblasts. Three batches of $Cspg2^{\Delta 3/\Delta 3}$ fibroblasts (M1, M2, and M3) and corresponding WT fibroblasts obtained from the same littermates were grown in DMEM containing 10% FBS. The $Cspg2^{\Delta 3/\Delta 3}$ fibroblasts appeared larger, flatter, and more spread out than WT fibroblasts in the growing phase at a low density and at confluence (Fig. 1*A*). The $Cspg2^{\Delta 3/\Delta 3}$ fibroblasts reached confluence more slowly than WT fibroblasts. At passage 5, they demonstrated ~50% BrdUrd incorporation as compared with that of WT fibroblasts at a comparable number of passages (Fig. 2*A*). The growth curve by counting the cells demonstrated slow growth of $Cspg2^{\Delta 3/\Delta 3}$ fibroblasts as compared with WT fibroblasts (Fig. 2*B*). To exclude the possibility that the slow proliferation of $Cspg2^{\Delta 3/\Delta 3}$ fibroblasts was due to a small population of proliferating cells, and a large one undergoing cell death, we examined levels of apoptosis. By DNA fragmentation assay, apoptosis was not observed in either WT or $Cspg2^{\Delta 3/\Delta 3}$ fibroblasts (data not shown).

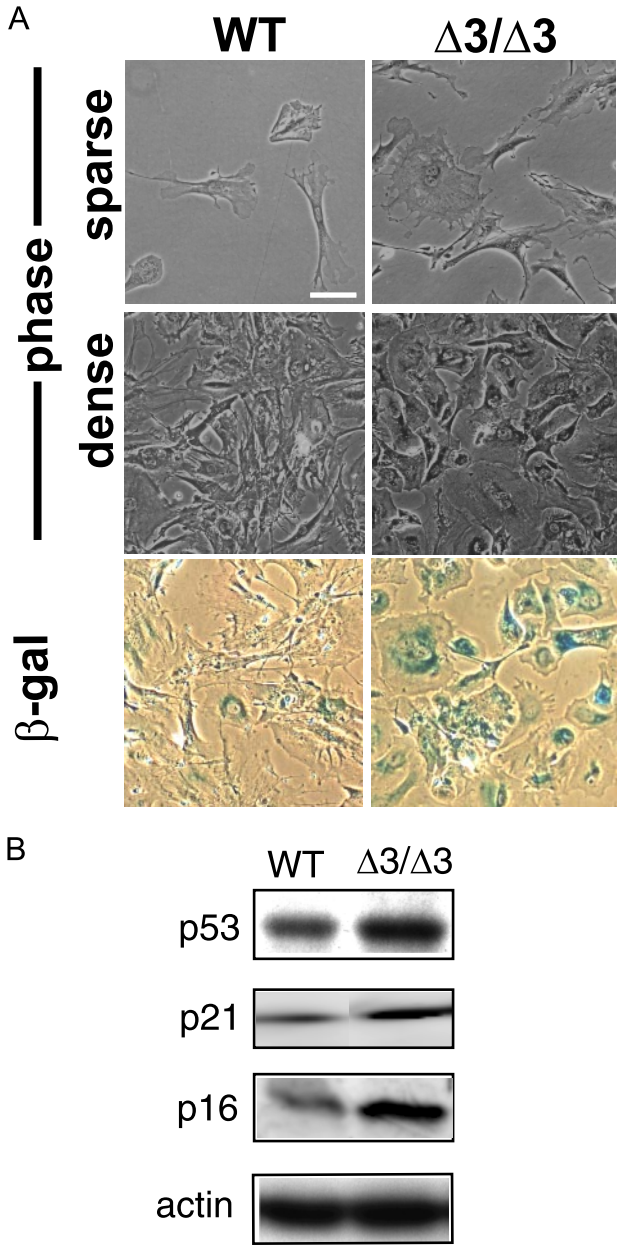

FIGURE 1. **Morphology and senescence of fibroblasts.** *A*, morphological changes and β-galactosidase (*β-gal*) staining patterns of wild type and the *Cspg2*$^{\Delta 3/\Delta 3}$ fibroblasts. WT and the *Cspg2*$^{\Delta 3/\Delta 3}$ (Δ3/Δ3) fibroblasts at a growing phase (sparse) and at day 1 after confluence (dense) are shown (*top four panels*). Staining patterns for β-galactosidase of these cells at day 1 after confluence are shown (*bottom two panels*). Note that the *Cspg2*$^{\Delta 3/\Delta 3}$ (Δ3/Δ3) fibroblasts are stained for β-galactosidase. *Bar*, 50 μm. *B*, immunoblot patterns of p53, p21, and p16. Note substantially elevated expression levels of them in the *Cspg2*$^{\Delta 3/\Delta 3}$ fibroblasts. The expression patterns of β-actin are also shown as standard. Staining for β-galactosidase was performed at least twice in three batches of *Cspg2*$^{\Delta 3/\Delta 3}$ fibroblasts and WT fibroblasts of the same littermates, and increased staining compared with WT was confirmed.

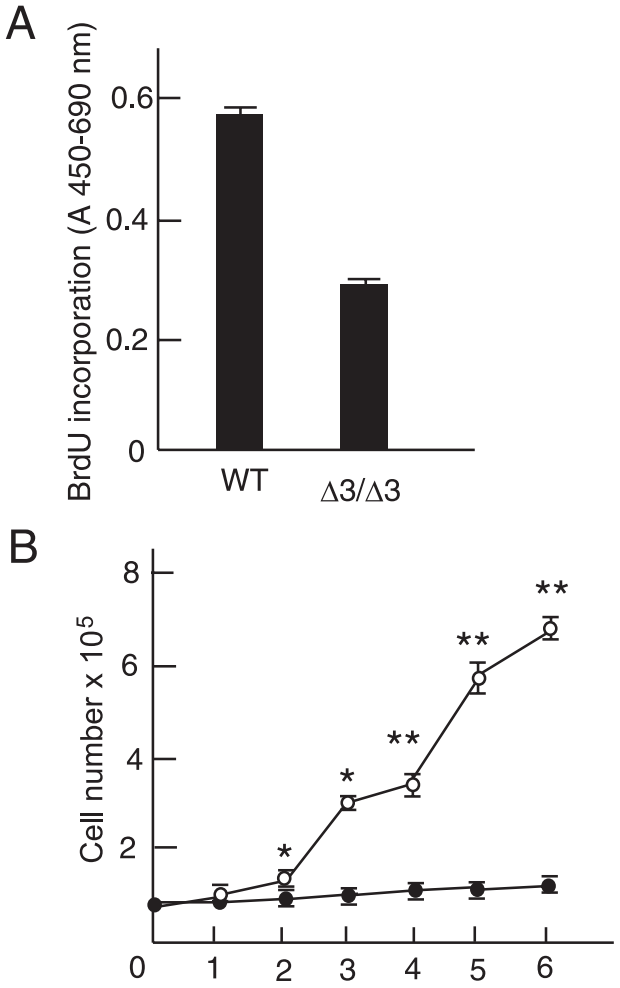

FIGURE 2. **Proliferation of wild type and the *Cspg2*$^{\Delta 3/\Delta 3}$ fibroblasts.** *A*, the rate of BrdUrd incorporation measured by A_{450} of WT and the *Cspg2*$^{\Delta 3/\Delta 3}$ (*Δ3/Δ3*) fibroblasts are shown. *B*, the cell number of these cells at growing phases is shown. The cells (1×10^5) were plated onto 6-well plates, and the cell number was counted as described under "Experimental Procedures" (*open circle*, WT; *closed circle*, *Cspg2*$^{\Delta 3/\Delta 3}$ fibroblasts). The *error bars* represent S.D. ($n = 3$). * and ** represent $p < 0.001$ and $p < 0.01$, respectively. Cell counting was performed at least twice in three batches of *Cspg2*$^{\Delta 3/\Delta 3}$ fibroblasts and WT fibroblasts of the same littermates. The data of M1 and corresponding WT fibroblasts are shown.

Cspg2$^{\Delta 3/\Delta 3}$ *Fibroblasts Exhibit Premature Senescence at Early Passages*—By staining for β-galactosidase indicative of the early phase of cell senescence, most *Cspg2*$^{\Delta 3/\Delta 3}$ fibroblasts exhibited intense staining, whereas only a few WT fibroblasts did (Fig. 1*A*). Thus, *Cspg2*$^{\Delta 3/\Delta 3}$ fibroblasts in early passages (<20 passages) appeared to undergo premature senescence. We further investigated the expression of markers for premature senescence, such as p53, p21, and p16. Immunoblot analysis revealed that their expression levels in *Cspg2*$^{\Delta 3/\Delta 3}$ fibroblasts were higher than those in WT fibroblasts (Fig. 1*B*), indicating that the *Cspg2*$^{\Delta 3/\Delta 3}$ fibroblasts acquired premature senescence.

Because cell shape and proliferation rate were similar among the three batches of *Cspg2*$^{\Delta 3/\Delta 3}$ and corresponding WT fibroblasts, and all of the *Cspg2*$^{\Delta 3/\Delta 3}$ fibroblast batches acquired premature senescence, we used M1 and WT fibroblasts from the same littermates, unless otherwise noted.

Versican Is Decreased in the Cspg2$^{\Delta 3/\Delta 3}$ *Fibroblasts*—Because senescence of *Cspg2*$^{\Delta 3/\Delta 3}$ fibroblasts was likely caused by the alteration of the ECM, we investigated distributions and levels of various ECM molecules known to regulate cell behavior. Initially, we examined the localization and the level of versican in the ECM. We plated WT and *Cspg2*$^{\Delta 3/\Delta 3}$ fibroblasts at an initial density of ~50 and ~70%, respectively. WT cells showed 100% confluence after 60 h. At 72 h, they showed a dense bundle network of versican in the ECM (Fig. 3*A*, *upper*

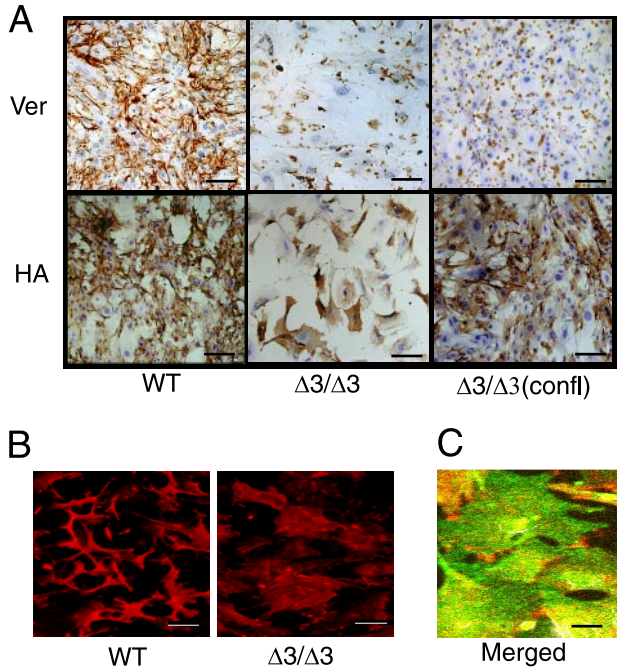

FIGURE 3. **Distributions of versican and hyaluronan.** *A*, immunostaining patterns of versican and HA are shown (*bar*, 100 μm). The cells were plated at an initial density of ~50% for WT and ~70% for *Cspg2*$^{\Delta3/\Delta3}$ fibroblasts. WT fibroblasts reached confluence at 60 h. At 72 h after the plating, *Cspg2*$^{\Delta3/\Delta3}$ fibroblasts reached ~90% confluence. Then both WT (*left panel*) and *Cspg2*$^{\Delta3/\Delta3}$ (*Δ3/Δ3*) fibroblasts (*middle panel*) were immunostained for versican (*Ver*, *top panels*) and HA (*bottom panels*). Separately, the *Cspg2*$^{\Delta3/\Delta3}$ fibroblasts plated at 100% confluence were grown for 48 h and immunostained for versican and HA (*right panel*, *confl*). Note scatter patterns of versican deposition in *Cspg2*$^{\Delta3/\Delta3}$ fibroblasts (*top middle* and *top right panels*) and that HA is localized on the cell surface of the *Cspg2*$^{\Delta3/\Delta3}$ fibroblasts (*bottom middle* and *bottom right panels*). *Bar*, 100 μm (except for *right top panel*, 250 μm). *B*, immunofluorescent staining patterns of HA. Note that HA was observed between cells in the ECM of WT (*left*), whereas it was localized on the cell surfaces in the *Cspg2*$^{\Delta3/\Delta3}$ fibroblast culture (*right*). *Bar*, 100 μm. *C*, double labeled fluorescent staining for HA and CD44 confirming localization of HA on the cell surfaces of the *Cspg2*$^{\Delta3/\Delta3}$ fibroblasts. *Bar*, 25 μm.

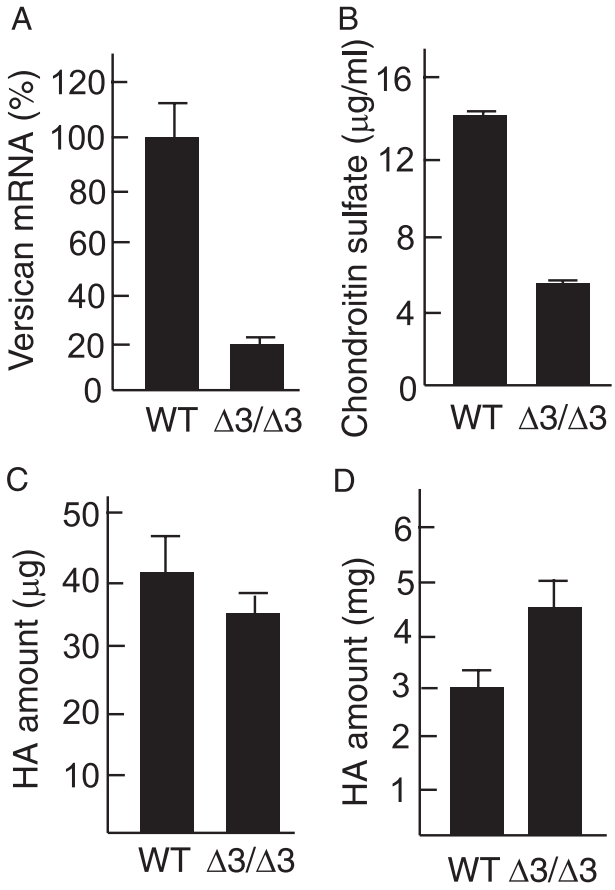

FIGURE 4. **Expression levels of versican and hyaluronan.** *A*, mRNA levels of versican gene. WT and *Cspg2*$^{\Delta3/\Delta3}$ (*Δ3/Δ3*) fibroblasts were plated at an initial density as above and grown for 72 h. Using these cells, reverse transcription-PCR was performed as described under "Experimental Procedures." The expression levels of versican standardized by glyceraldehyde-3-phosphate dehydrogenase expression are shown as a relative value. *Bar*, mean ± S.D. ($n = 3$). *B*, the levels of chondroitin sulfate in fibroblast culture. The cells were grown for 72 h as above, and then analysis was performed. *Δ3/Δ3*, the *Cspg2*$^{\Delta3/\Delta3}$ fibroblasts. *Bar*, mean ± S.D. ($n = 3$). *C*, the total levels of HA in the cell lysate and the ECM in fibroblast culture. *D*, the total levels of HA in the conditioned medium in fibroblast culture. *Δ3/Δ3*, the *Cspg2*$^{\Delta3/\Delta3}$ fibroblasts. The levels of HA were measured using the cells at 72 h after plating. *Bar*, mean ± S.D. ($n = 3$). Another set of identical experiments showed essentially the same results.

left panel). *Cspg2*$^{\Delta3/\Delta3}$ fibroblasts proliferated more slowly and reached ~90% confluence at 72 h. Then they showed scattered immunostaining patterns of versican (Fig. 3*A*, *upper middle panel*). When the *Cspg2*$^{\Delta3/\Delta3}$ fibroblasts were plated at 100% initial density and immunostained at 48 h, a similar scattered pattern of versican deposition was observed (Fig. 3*A*, *upper right panel*). Real time reverse transcription-PCR demonstrated that the levels of the mutant versican expression in the growing *Cspg2*$^{\Delta3/\Delta3}$ fibroblasts (at passages 5) decreased to ~25% that of normal versican in WT fibroblasts (Fig. 4*A*). Then we attempted to quantify deposition levels of versican. Because most chondroitin sulfate (CS) is derived from versican in proliferating fibroblasts,[5] we assumed that the amount of CS would reflect that of versican. The levels of CS in the ECM of the *Cspg2*$^{\Delta3/\Delta3}$ fibroblast culture were ~35% that in WT (Fig. 4*B*).

To confirm that the decreased versican deposition in the *Cspg2*$^{\Delta3/\Delta3}$ fibroblasts (Fig. 3*A*, *upper middle panel*) was not due to a decreased level of confluence, we examined the expression levels of other matrix molecules, such as fibronectin and laminin. Immunoblot analysis of WT and *Cspg2*$^{\Delta3/\Delta3}$ fibroblasts at 72 h revealed similar levels of these molecules (supplemental Fig. S2), and reference immunostaining indicated a similar pattern with the same intensity (data not shown). These results suggested that the substantial decrease of versican deposition was partly due to its diminished expression and partly due to the absence of the A subdomain.

HA Deposition Is Altered in Levels and Structure in the Cspg2$^{\Delta3/\Delta3}$ *Fibroblasts*—Because versican binds to HA at the B-B′ stretch of the G1 domain and the A subdomain of the G1 domain enhances the binding (3), decreased deposition of versican without the A subdomain in the *Cspg2*$^{\Delta3/\Delta3}$ presumably affects incorporation of HA in the ECM. Thus, we investigated the localization and expression levels of HA in these fibroblasts. When both cell types were plated at an initial density of 50 and 70%, respectively, and stained with biotinylated HA-binding protein at 72 h, HA was observed between cells in the ECM of WT (Fig. 3, *A*, *lower left panel*, and *B*, *left panel*), whereas it was faintly stained on the cell surfaces in the *Cspg2*$^{\Delta3/\Delta3}$ fibroblast culture (Fig. 3, *A*, *lower middle panel*, and *B*, *right panel*). Dou-

[5] S. Hatano, personal communication.

ble labeled fluorescent staining for HA and CD44 confirmed localization of HA on the cell surface (Fig. 3*C*). When the *Cspg2*$^{\Delta 3/\Delta 3}$ fibroblasts were plated at 100% initial density, and HA staining was performed at 48 h, HA was observed as dense bundles in the ECM and also on the cell surface (Fig. 3*A*, *lower right panel*). By enzyme-linked immunosorbent assay, the level of HA in the cell lysate, including the ECM of the *Cspg2*$^{\Delta 3/\Delta 3}$ culture at 90% confluence, was ~85% that of WT at 12 h after the confluence (Fig. 4*C*). In the *Cspg2*$^{\Delta 3/\Delta 3}$ fibroblast culture, the level of HA in the conditioned medium increased to ~1.5-fold (Fig. 4*D*), indicating that HA is less incorporated and more released in the conditioned medium. These observations suggested that the decreased versican deposition without the A subdomain altered HA matrix assembly in the *Cspg2*$^{\Delta 3/\Delta 3}$ fibroblasts.

MAPKs in Cspg2$^{\Delta 3/\Delta 3}$ *Fibroblasts*—To gain insight into the mechanisms underlying the acquisition of cell senescence in the *Cspg2*$^{\Delta 3/\Delta 3}$ fibroblasts by alteration of the ECM, we investigated phosphorylation and expression of signal transduction molecules. Immunoblot analysis of WT and *Cspg2*$^{\Delta 3/\Delta 3}$ fibroblasts at the confluence revealed a substantial increase in phosphorylation levels of ERK1/2 in the *Cspg2*$^{\Delta 3/\Delta 3}$ fibroblasts (passage ~5), as compared with those of WT fibroblasts. In contrast, phosphorylation levels of p38 MAPK and JNK/stress-activated protein kinase were similar between the two cell types (Fig. 5*A*). The levels of ERK1/2 phosphorylation were constant during proliferation, confluence, and 12 h after confluence in WT fibroblasts (data not shown). Increased phospho-ERK1/2 levels were confirmed in the other two batches of *Cspg2*$^{\Delta 3/\Delta 3}$ fibroblasts.

Next, we investigated whether the phosphorylation of ERK1/2 could be regulated by the upstream molecules of the signal transduction cascade (Fig. 5*B*). When treated with a MEK1 inhibitor PD98059, the level of phospho-ERK1/2 in WT fibroblasts substantially decreased, whereas the level in the *Cspg2*$^{\Delta 3/\Delta 3}$ fibroblasts, which had been higher than WT, decreased only slightly. When treated with EGF, the level of phophoERK1/2 in WT fibroblasts substantially increased, and that in the *Cspg2*$^{\Delta 3/\Delta 3}$ fibroblasts was no more elevated. These results suggested that the *Cspg2*$^{\Delta 3/\Delta 3}$ fibroblasts had the maximal level of ERK1/2 phosphorylation without EGF treatment.

The Extracellular Signal for ERK1/2 Phosphorylation Is Mediated by HA-CD44 Interaction—Our observations implied that the decreased levels of versican deposition, and altered levels and assembly of HA in the ECM caused constitutive phosphorylation of ERK1/2 in the *Cspg2*$^{\Delta 3/\Delta 3}$ fibroblasts, which may account for the premature senescence. Among the HA receptors on the cell surface, CD44 is known to mediate activation of ERK1/2 via Ras (30–32). Thus, we investigated whether the ERK1/2 phosphorylation was mediated by CD44 or not. By immunoblot analysis, the levels of CD44 expression were similar between WT and *Cspg2*$^{\Delta 3/\Delta 3}$ fibroblasts (data not shown). Immunostaining revealed nuclear localization of phospho-ERK1/2 in both cell types (Fig. 6*A*, *top panels*). When treated with an anti-CD44 antibody that blocks CD44-HA interaction, the staining intensity of individual nuclei was unaltered in the WT fibroblasts, whereas that in the *Cspg2*$^{\Delta 3/\Delta 3}$ fibroblasts was substantially diminished (Fig. 6*A*, *middle* and *bottom panels*).

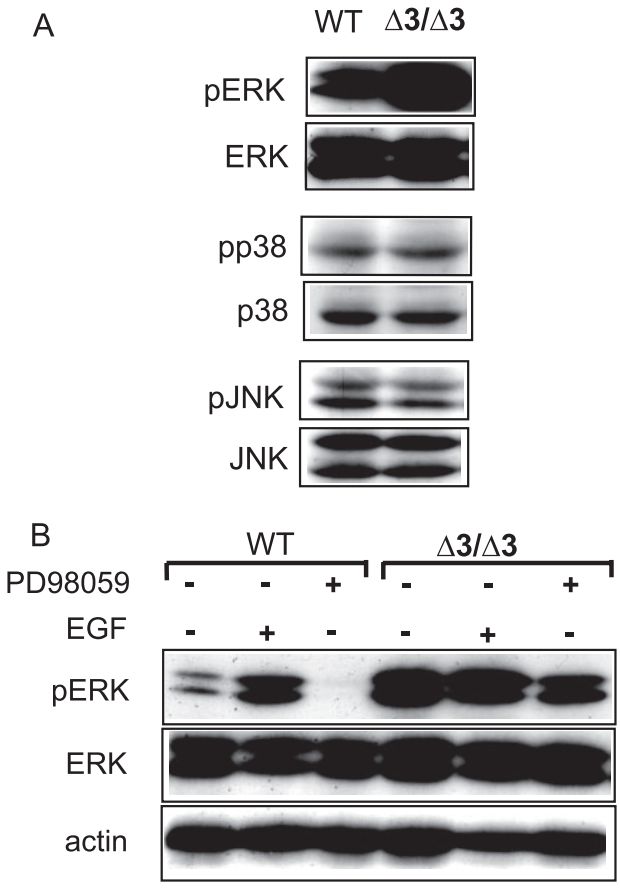

FIGURE 5. **Phosphorylation of MAPKs and expression of p53 in wild type and *Cspg2*$^{\Delta 3/\Delta 3}$ fibroblasts.** *A*, immunoblot patterns of ERK1/2 (*ERK*), p38 MAPK (*p38*), and JNK and their phosphorylated molecules. *Δ3/Δ3*, the *Cspg2*$^{\Delta 3/\Delta 3}$ fibroblasts. WT and *Cspg2*$^{\Delta 3/\Delta 3}$ fibroblasts were plated at a density of ~50 and ~70%, respectively, and grown up to confluence. Then the culture medium was replaced with DMEM containing 1% FBS and further cultured for 18 h. Immunoblot analyses were performed as described under "Experimental Procedures." Note dramatically elevated levels of phospho-ERK1/2 in *Cspg2*$^{\Delta 3/\Delta 3}$ fibroblasts. *B*, effects of PD98059 and EGF on phosphorylation of ERK1/2. The fibroblasts at confluence were cultured in DMEM containing 1% FBS. The cells were treated with EGF (20 μg/ml) for 2 h or with PD98059 (30 mM) for 1 h, and at 18 h, cells were collected and used for immunoblot analysis.

These results suggested that HA-CD44 interaction elevated phosphorylation levels of ERK1/2 in the *Cspg2*$^{\Delta 3/\Delta 3}$ fibroblasts.

Increased HA-CD44 interaction in the *Cspg2*$^{\Delta 3/\Delta 3}$ fibroblasts contrasts with the decreased incorporation of HA in the ECM. We speculated that the ECM of the *Cspg2*$^{\Delta 3/\Delta 3}$ fibroblast culture was loosely organized, and the free HA chains were more accessible to the cell surface. Actually, HA was stained on the cell surface of *Cspg2*$^{\Delta 3/\Delta 3}$ fibroblasts (Fig. 3*A*, *lower middle panel*). To test this hypothesis, we treated WT fibroblasts with hyaluronidase and examined its effects on ERK1/2 phosphorylation. Immunoblot analysis demonstrated a significant increase in ERK1/2 phosphorylation by hyaluronidase treatment for 30 min and 2 h at concentrations of both 0.2 and 2 mg/ml (Fig. 6, *B* and *C*). In addition, combined treatment with hyaluronidase (0.2 mg/ml) and the anti-CD44 antibody attenuated phospho-ERK1/2 levels to ~60% by the antibody (Fig. 6*D*). This inhibition was not observed when the anti-CD44 antibody was replaced with an antibody that does not block CD44-HA interaction (data not shown). These results suggested that hyalu-

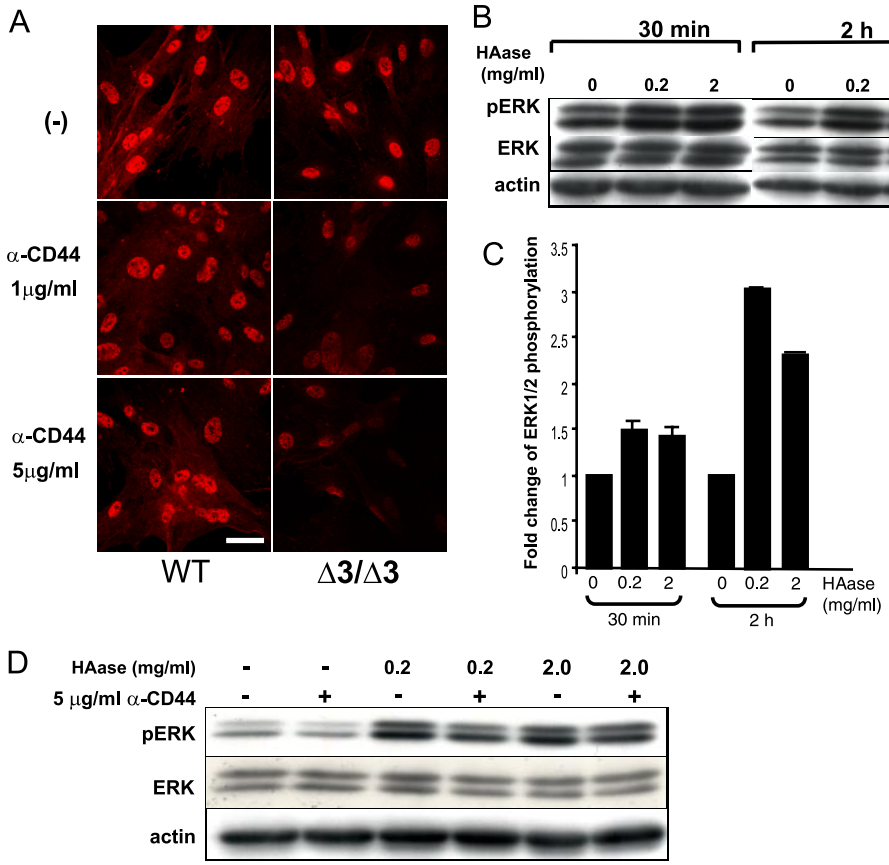

FIGURE 6. **Effects of hyaluronidase treatment and blocking of HA-CD44 interaction on phosphorylation of ERK1/2.** *A*, effects of anti-CD44 treatment on phospho-ERK1/2. Immunostaining patterns for phospho-ERK1/2 are shown. *Δ3/Δ3*, the *Cspg2*$^{\Delta3/\Delta3}$ fibroblasts. Both WT and the *Cspg2*$^{\Delta3/\Delta3}$ fibroblasts were cultured in the presence of an anti-CD44 antibody that blocks HA-CD44 interaction at 1 or 5 μg/ml, as described under "Experimental Procedures." Note that treatment with the antibody substantially diminishes the staining intensity for phospho-ERK1/2 in the *Cspg2*$^{\Delta3/\Delta3}$ fibroblasts (*bar*, 20 μm). *B*, effects of hyaluronidase treatment on phosphorylation of ERK1/2 in WT fibroblasts. The cells were treated for the periods at the concentrations of hyaluronidase (*HAase*) as indicated and applied to immunoblot analysis to detect phospho-ERK1/2 (*pERK*), total ERK1/2 (*ERK*), and actin. *C*, phosphorylation levels of ERK1/2. The band density was quantified using a densitometer. That of phospho-ERK1/2 standardized by that of total ERK1/2 is shown. *D*, effects of combined treatment with hyaluronidase and anti-CD44. The cells were treated with combinations of hyaluronidase and anti-CD44 (*α-CD44*) for 2 h at the concentrations indicated and applied to immunoblot analysis to detect phospho-ERK1/2 (*pERK*), total ERK1/2 (*ERK*), and actin.

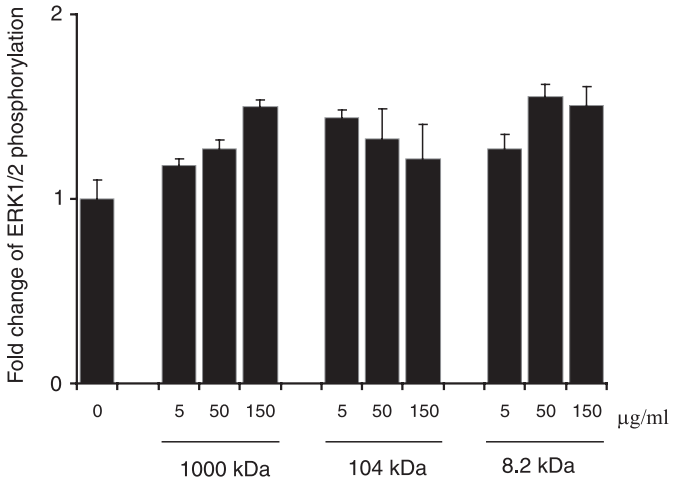

FIGURE 7. **Effects of exogenous hyaluronan on phosphorylation of ERK1/2.** WT fibroblasts at confluence were treated with different molecular sizes of HA at the concentrations indicated for 16 h, and the cell lysates were applied to immunoblot analysis for phospho-ERK1/2 and total ERK1/2. The band density quantified by densitometry is indicated as fold changes of phophoERK1/2. The values are the means ± S.E. ($n = 2$). The experiments were performed twice, and essentially the same results were obtained.

ronidase treatment liberated HA fragments from the ECM, and the fragments transmitted the signal by binding to CD44.

Exogenous HA Treatment Enhances Phosphorylation of ERK1/2—Our observations strongly suggested that decreased versican inhibited HA-associated matrix assembly and liberated free HA, which in turn facilitated its interaction with CD44 leading to phosphorylation of ERK1/2. To test this hypothesis, we treated WT fibroblasts with different sizes of HA and examined phosphorylation levels of ERK1/2. Immunoblot analysis revealed that phosphorylation of ERK1/2 was elevated by the treatment with all sizes of HA (Fig. 7). Thus, it was likely that interaction of free HA fragments with CD44 enhanced ERK1/2 phosphorylation.

Versican has been shown to stimulate proliferation of NIH3T3 cells (23). Recent studies have revealed that the versican G3 domain interacts with β1-integrin which, in turn, interferes with β1-integrin-EGF receptor interaction (22). Immunoblot analysis showed that the expression levels of β1-integrin and EGF receptor were similar between WT and the *Cspg2*$^{\Delta3/\Delta3}$ fibroblasts. In addition, the phosphorylation level of the EGF receptor was also similar between the two (data not shown). Thus, it is unlikely that decreased versican directly attenuated cell proliferation by affecting signal transduction pathways involving β1-integrin and EGFR.

DISCUSSION

In this study, we have demonstrated that *Cspg2*$^{\Delta3/\Delta3}$ fibroblasts, whose versican lacks the A subdomain of the G1 domain, grow more slowly than WT fibroblasts and acquire cellular senescence. In culture of *Cspg2*$^{\Delta3/\Delta3}$ fibroblasts, the disorganized HA matrix by decreased versican deposition and HA chains released in the conditioned medium, enhance CD44-mediated signal transduction, leading to constitutively active ERK1/2 and premature senescence. This study illustrates that the altered matrix structure, involving versican and HA, causes premature senescence. Our results demonstrate the pivotal role of the extracellular matrix structure in the regulation of cell behavior.

The level of versican mRNA and that of CS in the senescent *Cspg2*$^{\Delta3/\Delta3}$ fibroblasts was substantially decreased, presumably because of both a decreased transcription level caused by inser-

tion of *neo*^{r} gene into exon 3 and a lack of the A subdomain, which enhances interaction of versican with HA (3). The decreased expression of the mutant versican with reduced HA binding affinity in the *Cspg2*$^{\Delta3/\Delta3}$ fibroblasts possibly affects HA deposition. In WT fibroblast culture, HA exhibited a network structure together with versican, whereas in the *Cspg2*$^{\Delta3/\Delta3}$ fibroblast culture, it did not show such a network structure. Although the *Cspg2*$^{\Delta3/\Delta3}$ fibroblast culture showed substantially decreased staining for HA, the deposition level of HA was decreased only to ~85%. Thus, versican may function to assemble HA chains into a network as well as to maintain the HA level in the ECM. The G3 domain of versican and aggrecan binds various ECM molecules including fibulins (7), known to form dimers that act as cross-linkers between different HA-aggrecan complexes. They may similarly form HA-versican complexes and facilitate assembly of HA chains to fibrils. Decreased versican deposition in *Cspg2*$^{\Delta3/\Delta3}$ fibroblast culture may abrogate formation of the complex that facilitates the HA assembly. Recent studies have revealed that HA can be present in many structural forms, exhibiting specific functions (33). For example, when cultured colon smooth muscle cells are treated with a viral mimetic, poly(I-C), they exhibit HA with a cable structure, which has presumably formed from coalescence of smaller HA strands. Monocytes recognize and bind the HA cable structure but not the HA patches (34). Furthermore, we recently demonstrated that SHAP (serum-derived hyaluronan-associated protein) potentiates CD44-mediated leukocyte adhesion to the HA substratum, suggesting that SHAP organizes the HA structure (35). Our results may provide another line of evidence that HA in an organized structure regulates cell behavior.

Treatment of *Cspg2*$^{\Delta3/\Delta3}$ fibroblasts with an anti-CD44 antibody that blocks HA-CD44 interaction substantially decreased phosphorylation of ERK1/2. CD44 is known to activate ERK1/2 in some cell culture systems. Treatment of proximal tubular cells with HA transduces a signal via CD44, activates ERK1/2, and promotes cell migration (36). Heparan sulfate-modified CD44 binds hepatocyte growth factor/scatter factor and promotes receptor tyrosine kinase (RTK)-mediated signal transduction (32). In our experiments, treatment of the *Cspg2*$^{\Delta3/\Delta3}$ fibroblasts with a MEK1 inhibitor PD98059 attenuated the phosphorylation of ERK1/2 to a certain extent, whereas treatment with EGF did not attain further phosphorylation. These results indicate that full activation of ERK1/2 is achieved by the signal induced from the altered ECM and that the activation can be regulated by the RTK. Recent studies have revealed that a CD44v6 variant form physically interacts with RTKs and activates them (31). The link between CD44 and RTKs remains to be studied.

Oncogenic Ras is known to induce premature senescence in primary fibroblasts (37). Although several Ras-dependent signaling pathways have been identified, constitutively active Ras-Raf-MEK-ERK1/2 cascade, or even active MEK, is sufficient for premature senescence (38). Cellular senescence is accompanied by up-regulated expression of p53, p16, and p21 and accumulation of senescence-associated β-galactosidase (SA-β-gal). The *Cspg2*$^{\Delta3/\Delta3}$ fibroblasts showed a high phosphorylation level of ERK1/2, which is indicative of constitutively active MEK. In addition, they exhibited up-regulated expression of these senescence markers and positive staining for β-galactosidase. All of these observations suggest that premature senescence in the *Cspg2*$^{\Delta3/\Delta3}$ fibroblasts is due to constitutively active ERK1/2.

HA is known to exhibit different effects on cell behavior, dependent on its size and whether or not it is incorporated into the extracellular matrix. For example, endogenous HA transduces a signal via interaction with CD44 and that the HA oligosaccharides competitively inhibit their interaction and down-regulate the signal (39, 40). In this study, we have shown that hyaluronidase treatment increased phospho-ERK1/2 levels in WT fibroblasts, which was partially inhibited by blocking the interaction of HA with CD44 using a specific anti-CD44 antibody. Surprisingly, treatment of NIH3T3 fibroblasts with hyaluronidase similarly enhanced phosphorylation of ERK1/2, suggesting that the HA-mediated ERK1/2 activation is conserved among mouse fibroblastic cell types.[6] In addition, treatment with HA fragments substantially elevated the phospho-ERK1/2 levels. These observations strongly suggest that free HA chains, rather than those incorporated into the matrix, transduce the CD44-mediated signal, leading to phosphorylation of ERK1/2. Interestingly, HA with a size of ~1,000 kDa increased the phospho-ERK1/2 levels in a dose-dependent manner, whereas HA with a size of ~104 kDa had the highest phospho-ERK1/2 level at a concentration of 5 μg/ml. Other factors may be involved in the accessibility, local concentration, and the optimal signal transduction of HA.

Previous studies have shown some effects of versican domains on cell behavior via EGFR. The G3 domain of versican enhances proliferation of NIH3T3 fibroblasts via EGF-like motifs (23). The G3 domain without the EGF-like motifs enhances EGFR/β1-integrin association and attenuates EGFR phosphorylation in U87 astrocytoma cells, thus impairing the autonomous growth of the cells (22). The V1 variant enhances proliferation of NIH3T3 cells by up-regulating EGFR expression, whereas the V2 variant exhibits an opposite activity (20). Our immunoblot analysis revealed similar expression levels of β1-integrin in WT and the *Cspg2*$^{\Delta3/\Delta3}$ fibroblasts. The phosphorylation level of EGFR was the same in both cell types. These observations, which contrast with the previous data, suggest that the versican G3 domain is unlikely to directly affect proliferation in *Cspg2*$^{\Delta3/\Delta3}$ fibroblast cultures.

In conclusion, our results clearly demonstrate the pivotal role of the ECM structure, involving versican and HA, in the acquisition of premature senescence. In inflammation and repair processes, fibroblasts migrate, proliferate, and then cease to grow during reorganization of the tissue. Experimental wound healing models in conditional knock-out mice of versican would facilitate understanding the roles of versican and HA in these processes. This study provides a clue to the regulation of inflammation and repair processes by manipulating ECM molecules.

Acknowledgment—We thank S. Hara for technical assistance.

REFERENCES

1. Zimmermann, D. R., and Ruoslahti, E. (1989) *EMBO J.* **8,** 2975–2981
2. Shinomura, T., Nishida, Y., Ito, K., and Kimata, K. (1993) *J. Biol. Chem.*

[6] K. Choocheep, unpublished data.

268, 14461–14469
3. Matsumoto, K., Shionyu, M., Go, M., Shimizu, K., Shinomura, T., Kimata, K., and Watanabe, H. (2003) *J. Biol. Chem.* **278,** 41205–41212
4. Wu, Y. J., La Pierre, D. P., Wu, J., Yee, A. J., and Yang, B. B. (2005) *Cell Res.* **15,** 483–494
5. Isogai, Z., Aspberg, A., Keene, D. R., Ono, R. N., Reinhardt, D. P., and Sakai, L. Y. (2002) *J. Biol. Chem.* **277,** 4565–4572
6. Aspberg, A., Adam, S., Kostka, G., Timpl, R., and Heinegard, D. (1999) *J. Biol. Chem.* **274,** 20444–20449
7. Olin, A. I., Morgelin, M., Sasaki, T., Timpl, R., Heinegard, D., and Aspberg, A. (2001) *J. Biol. Chem.* **276,** 1253–1261
8. Aspberg, A., Binkert, C., and Ruoslahti, E. (1995) *Proc. Natl. Acad. Sci. U. S. A.* **92,** 10590–10594
9. Suwiwat, S., Ricciardelli, C., Tammi, R., Tammi, M., Auvinen, P., Kosma, V. M., LeBaron, R. G., Raymond, W. A., Tilley, W. D., and Horsfall, D. J. (2004) *Clin. Cancer Res.* **10,** 2491–2498
10. Tsujii, M., Hirata, H., Yoshida, T., Imanaka-Yoshida, K., Morita, A., and Uchida, A. (2006) *Histol. Histopathol.* **21,** 511–518
11. Yamagata, M., Yamada, K. M., Yoneda, M., Suzuki, S., and Kimata, K. (1986) *J. Biol. Chem.* **261,** 13526–13535
12. Yamagata, M., and Kimata, K. (1994) *J. Cell Sci.* **107,** 2581–2590
13. Braunewell, K. H., Pesheva, P., McCarthy, J. B., Furcht, L. T., Schmitz, B., and Schachner, M. (1995) *Eur. J. Neurosci.* **7,** 805–814
14. Mazzucato, M., Cozzi, M. R., Pradella, P., Perissinotto, D., Malmstrom, A., Morgelin, M., Spessotto, P., Colombatti, A., De Marco, L., and Perris, R. (2002) *FASEB J.* **16,** 1903–1916
15. Landolt, R. M., Vaughan, L., Winterhalter, K. H., and Zimmermann, D. R. (1995) *Development* **121,** 2303–2312
16. Evanko, S. P., Angello, J. C., and Wight, T. N. (1999) *Arterioscler. Thromb. Vasc. Biol.* **19,** 1004–1013
17. Perissinotto, D., Iacopetti, P., Bellina, I., Doliana, R., Colombatti, A., Pettway, Z., Bronner-Fraser, M., Shinomura, T., Kimata, K., Morgelin, M., Lofberg, J., and Perris, R. (2000) *Development* **127,** 2823–2842
18. Cattaruzza, S., Schiappacassi, M., Kimata, K., Colombatti, A., and Perris, R. (2004) *FASEB J.* **18,** 779–781
19. Hinek, A., Braun, K. R., Liu, K., Wang, Y., and Wight, T. N. (2004) *Am. J. Pathol.* **164,** 119–131
20. Sheng, W., Wang, G., Wang, Y., Liang, J., Wen, J., Zheng, P. S., Wu, Y., Lee, V., Slingerland, J., Dumont, D., and Yang, B. B. (2005) *Mol. Biol. Cell* **16,** 1330–1340
21. Domenzain, C., Docampo, M. J., Serra, M., Miquel, L., and Bassols, A. (2003) *Biochim. Biophys. Acta* **1642,** 107–114
22. Wu, Y., Chen, L., Cao, L., Sheng, W., and Yang, B. B. (2004) *J. Cell Sci.* **117,** 2227–2237
23. Zhang, Y., Cao, L., Yang, B. L., and Yang, B. B. (1998) *J. Biol. Chem.* **273,** 21342–21351
24. Mjaatvedt, C. H., Yamamura, H., Capehart, A. A., Turner, D., and Markwald, R. R. (1998) *Dev. Biol.* **202,** 56–66
25. Hogan, B., Beddington, R., Constantini, F., and Lacy, E. (1994) *Manipulating the Mouse Embryo*, pp. 260–261, Cold Spring Harbor Laboratory, Cold Spring Harbor, NY
26. Dimri, G. P., Lee, X., Basile, G., Acosta, M., Scott, G., Roskelley, C., Medrano, E. E., Linskens, M., Rubelj, I., and Pereira-Smith, O. (1995) *Proc. Natl. Acad. Sci. U. S. A.* **92,** 9363–9367
27. Matsumoto, K., Kamiya, N., Suwan, K., Atsumi, F., Shimizu, K., Shinomura, T., Yamada, Y., Kimata, K., and Watanabe, H. (2006) *J. Biol. Chem.* **281,** 18257–18263
28. Kimata, K., Sakakura, T., Inaguma, Y., Kato, M., and Nishizuka, Y. (1985) *J. Embryol. Exp. Morphol.* **89,** 243–257
29. Kamiya, N., Watanabe, H., Habuchi, H., Takagi, H., Shinomura, T., Shimizu, K., and Kimata, K. (2006) *J. Biol. Chem.* **281,** 2390–2400
30. Bourguignon, L. Y., Gilad, E., Brightman, A., Diedrich, F., and Singleton, P. (2006) *J. Biol. Chem.* **281,** 14026–14040
31. Cheng, C., Yaffe, M. B., and Sharp, P. A. (2006) *Genes Dev.* **20,** 1715–1720
32. van der Voort, R., Taher, T. E., Wielenga, V. J., Spaargaren, M., Prevo, R., Smit, L., David, G., Hartmann, G., Gherardi, E., and Pals, S. T. (1999) *J. Biol. Chem.* **274,** 6499–6506
33. Hascall, V. C., Majors, A. K., De La Motte, C. A., Evanko, S. P., Wang, A., Drazba, J. A., Strong, S. A., and Wight, T. N. (2004) *Biochim. Biophys. Acta* **1673,** 3–12
34. Majors, A. K., Austin, R. C., de la Motte, C. A., Pyeritz, R. E., Hascall, V. C., Kessler, S. P., Sen, G., and Strong, S. A. (2003) *J. Biol. Chem.* **278,** 47223–47231
35. Zhuo, L., Kanamori, A., Kannagi, R., Itano, N., Wu, J., Hamaguchi, M., Ishiguro, N., and Kimata, K. (2006) *J. Biol. Chem.* **281,** 20303–20314
36. Ito, T., Williams, J. D., Al-Assaf, S., Phillips, G. O., and Phillips, A. O. (2004) *Kidney Int.* **65,** 823–833
37. Serrano, M., Lin, A. W., McCurrach, M. E., Beach, D., and Lowe, S. W. (1997) *Cell* **88,** 593–602
38. Lin, A. W., Barradas, M., Stone, J. C., van Aelst, L., Serrano, M., and Lowe, S. W. (1998) *Genes Dev.* **12,** 3008–3019
39. Camenisch, T. D., Spicer, A. P., Brehm-Gibson, T., Biesterfeldt, J., Augustine, M. L., Calabro, A., Jr., Kubalak, S., Klewer, S. E., and McDonald, J. A. (2000) *J. Clin. Investig.* **106,** 349–360
40. Tsatas, D., Kanagasundaram, V., Kaye, A., and Novak, U. (2002) *J. Clin. Neurosci.* **9,** 282–288